higher than those of **1**-Zn ($1.4 \times 10^4\,\text{M}^{-1}$) and **1**-Co ($7.2 \times 10^4\,\text{M}^{-1}$) under the same conditions.

[14] ^{13}C NMR ($CDCl_3$, 25 °C) of bipyridine: $\delta = 150.3$ (C2), 121.1 (C3), 145.2 (C4); **1**-RhMe ⊃ bipyridine: $\delta = 144.2$ (C2), 117.9 (C3), 140.7 (C4).

[15] ^{13}C NMR ($CDCl_3/CS_2$ 1:1): C_{70} (equator to pole) at 25 °C: $\delta = 130.4$, 144.9, 147.6, 146.9, 150.1; at −60 °C: $\delta = 130.0$, 144.5, 147.2, 146.5, 149.7; C_{70}/**1**-Zn (1:2) at 25 °C: $\delta = 126.6$ ($\Delta\delta = -3.8$), 141.3 (−3.6), 144.5 (−3.1), 144.2 (−2.7), 147.7 (−2.4); at −60 °C: $\delta = 125.9$ ($\Delta\delta = -4.1$), 140.7 (−3.8), 143.9 (−3.3), 143.7 (−2.8), 147.2 (−2.5).

[16] R. Taylor, J. P. Hare, A. K. Abdul-Sada, H. W. Kroto, *J. Chem. Soc. Chem. Commun.* **1990**, 1423.

[17] T. Haino, M. Yanase, Y. Fukazawa, *Angew. Chem.* **1998**, *110*, 1044; *Angew. Chem. Int. Ed.* **1998**, *37*, 997.

[18] ^{13}C NMR ($CDCl_3/CS_2$ 1:1) of C_{70}/**1**-RhMe (1:2) (equator to pole) at 25 °C: $\delta = 126.8$ ($\Delta\delta = -3.6$), 141.2 (−3.7), 144.2 (−3.4), 143.8 (−3.1), 147.1 (−3.0); at −60 °C: $\delta = 126.5$ ($\Delta\delta = -3.9$), 141.0 (−3.9), 143.6 (−4.0), 142.7 (−4.2), 146.0 (−4.1).

[19] Selective coordination of Pt^0 and Ir^I to C_{70} at 6:6 ring junctions close to the pole has been reported: a) A. L. Balch, V. J. Catalano, J. W. Lee, M. M. Olmstead, S. R. Parkin, *J. Am. Chem. Soc.* **1991**, *113*, 8953; b) A. L. Balch, L. Hao, M. M. Olmstead, *Angew. Chem.* **1996**, *108*, 211; *Angew. Chem. Int. Ed. Engl.* **1996**, *35*, 188.

[20] Chemical shifts of C_{60} and C_{70} at 20 and 60 °C, respectively, in the presence of excess amounts of **1**-Zn (C_{60}/**1**-Zn = 1:5, C_{70}/**1**-Zn = 1:2.4) were used.

[21] Estimated on the basis of the coalescence profile of a ^{13}C NMR signal of the carbon atoms on the pole of C_{70}.

[22] J. K. M. Sanders, B. K. Hunter, *Modern NMR Spectroscopy*, Oxford University Press, Oxford, **1987**.

[23] a) B. Wayland, S. L. Van Voorhees, K. J. Del Rossi, *J. Am. Chem. Soc.* **1987**, *109*, 6513; b) J. L. Maxwell, K. C. Brown, D. W. Bartley, T. Kodadek, *Science* **1992**, *256*, 1544.

[24] $K_{assoc} = 1.4 \times 10^6\,\text{M}^{-1}$ for C_{60} and $2.4 \times 10^7\,\text{M}^{-1}$ for C_{70} in benzene at 25 °C.

[25] Almost comparable to the association constant of a quadruple hydrogen bonding interaction, usable for the construction of supramolecular polymers: B. J. B. Folmer, R. P. Sijbesma, H. Kooijman, A. L. Spek, E. M. Meijer, *J. Am. Chem. Soc.* **1999**, *121*, 9001.

Photoelectrochemistry with Controlled DNA-Cross-Linked CdS Nanoparticle Arrays**

Itamar Willner,* Fernando Patolsky, and Julian Wasserman

Electronics based on DNA has been the subject of extensive recent research activities that address the conductivity features of double-stranded (ds) DNA,[1–7] the use of ds-DNA as a template for the construction of nanowires,[8] and the employment of metal nanoparticles cross-linked by DNA as single-electron charging devices.[9, 10] The optical properties of DNA-cross-linked Au nanoparticles were recently studied and applied for DNA sensing,[11, 12] and nanoarchitectures of DNA/Au nanoparticles were assembled.[13] The electronic transduction of DNA sensing and, in particular, amplified DNA analyses were recently studied by using electrochemical measurements[14–23] or microgravimetry[16] with a quartz-crystal microbalance. Direct electrochemical detection of DNA was achieved by monitoring the electrochemical response of DNA[14–16] or by the incorporation of redox-labels into ds-DNA.[17–19] The amplified detection of DNA was accomplished by the use of biocatalytic conjugates[20, 21] and the application of labeled liposomes[22, 23] or nanoparticles.[24, 25]

Herein we describe the novel architecture of double-stranded DNA-cross-linked CdS nanoparticle arrays on electrode supports and the structurally controlled generation of photocurrents upon irradiation of these arrays. The electrostatic binding of $[Ru(NH_3)_6]^{3+}$ to the ds-DNA units provides tunneling routes for the conduction-band electrons and thus results in enhanced photocurrents. Besides the unique and novel photoelectrochemical features of the systems, the assemblies provide a new means for the optical fluorescence and electronic (photoelectrochemical) transduction of DNA-sensing events.

CdS nanoparticles (2.6 ± 0.4 nm) were functionalized with thiolated oligonucleotide **1** or **2**. These two oligonucleotides are complementary to the 5′- and 3′-ends of the target DNA **3**. The size of the CdS nanoparticles was determined from HR-transmission electron microscopy (TEM) images (average of 150 particles). Using the absorption spectra of the CdS nanoparticles ($\lambda_{max} = 405$ nm) and the Brus equation[26] gave a similar particle size. We estimate that about 20–24 oligonucleotide units are associated with each CdS nanoparticle (see *Experimental Section* for details). Figure 1 shows the stepwise assembly of the DNA-cross-linked CdS particles on an Au electrode. The oligonucleotide **1** was assembled on the Au electrode ($2.3 \times 10^{-11}\,\text{mol cm}^{-2}$) and then treated with the analyte **3** to yield the ds system. Subsequent interaction of the surface with the **2**-functionalized CdS resulted in the binding of the CdS nanoparticles to the surface. Further alternating interaction of the interface with a solution containing the **1**-functionalized CdS nanoparticles ($1\,\text{mg mL}^{-1}$) pretreated with **3** (1×10^{-6} M) and with a solution containing **2**-functionalized CdS nanoparticles resulted in an array with a controlled number of CdS nanoparticle generations. The buildup of the DNA-cross-linked CdS nanoparticle array was monitored by microgravimetry with a quartz-crystal microbalance (Figure 2A).

From the frequency changes observed upon the buildup of the first generation of CdS nanoparticles, and knowing their dimensions, we estimate the surface coverage to be about 1.6×10^{12} particles per square centimeter. This value corresponds to around 15% of a densely packed particle layer. The negative charge associated with the nucleic acid functionalized nanoparticles probably prevents the formation of a dense particle configuration. The DNA-cross-linked CdS nanoparticle arrays were also assembled on glass supports by using an aminopropylsiloxane-functionalized glass that was treated with ε-maleimidocaproic *N*-hydroxysuccinimide ester[24, 25] as a base interface for the covalent linkage of **1** and the organization of the nanoparticle systems. Figure 2B shows

[*] I. Willner, F. Patolsky, J. Wasserman
The Institute of Chemistry and
The Farkas Center for Light-Induced Processes
The Hebrew University of Jerusalem
Jerusalem 91904 (Israel)
Fax (+972) 2-6527715
E-mail: willnea@vms.huji.ac.il

[**] This research is supported by The U.S.–Israel Binational Science Foundation. The Max Planck Research Award for International Cooperation (I.W.) is gratefully acknowledged.

Supporting information for this article is available on the WWW under http://www.angewandte.com or from the author.

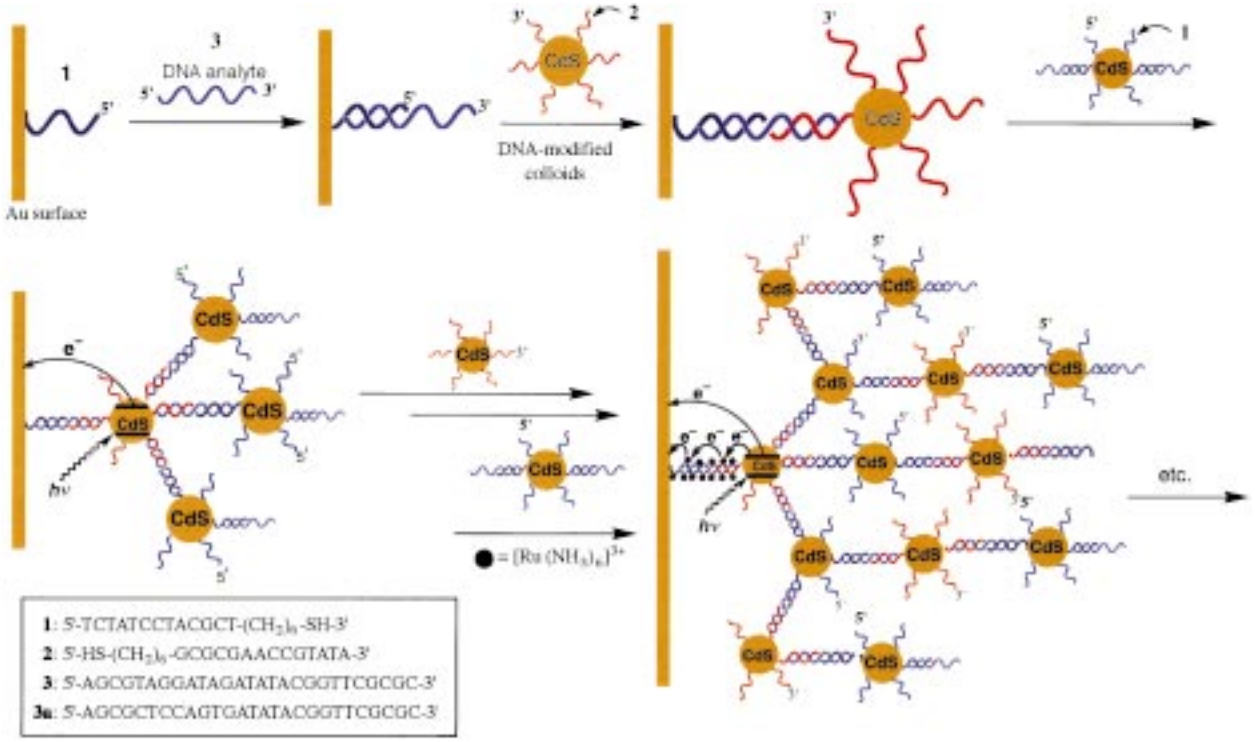

Figure 1. The organization of oligonucleotide/DNA-cross-linked arrays of CdS nanoparticles and the photoelectrochemical response of the nanoarchitectures.

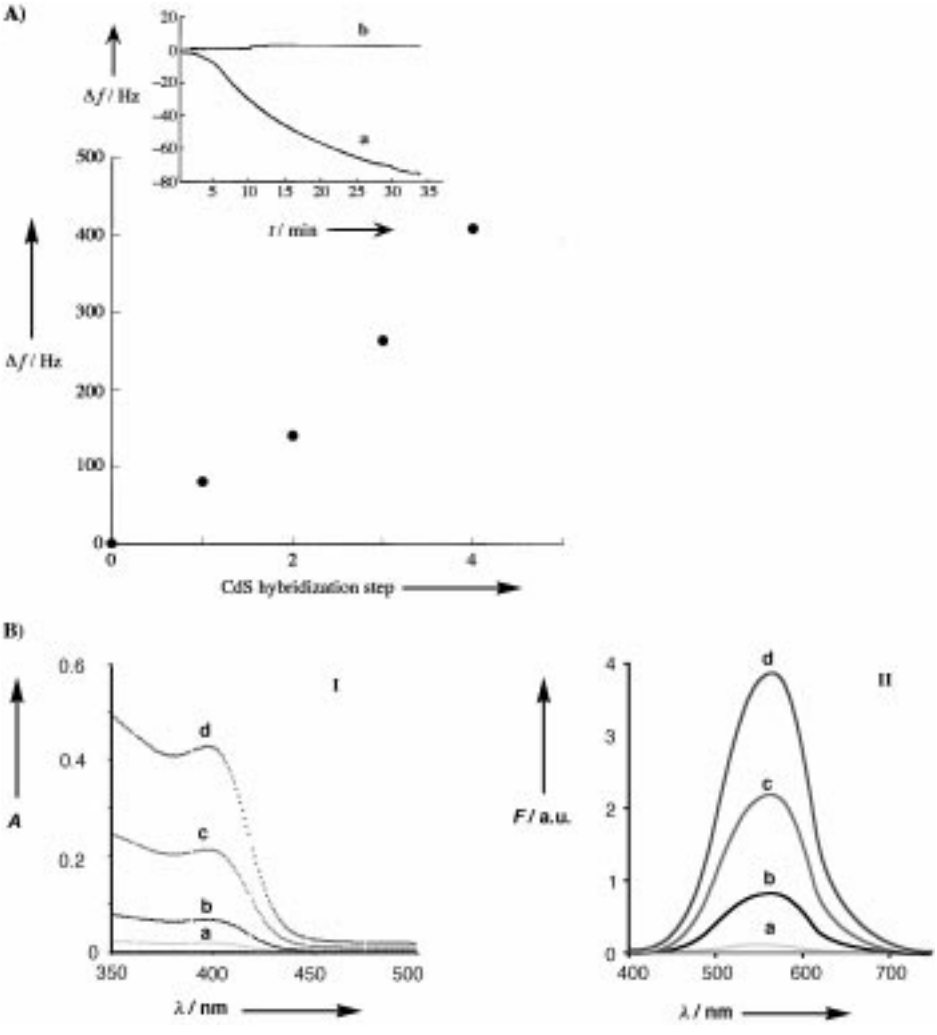

Figure 2. A) The frequency change of an Au/quartz crystal in air (9 MHz, AT-cut) upon the assembly of oligonucleotide/DNA-cross-linked CdS nanoparticle layers. The first layer was assembled by the reaction of the **1**-functionalized electrode with **3** (1×10^{-6} M) and then with the **2**-modified CdS nanoparticles. The other layers were constructed by the alternating treatment of the surface with a solution of **3** (1×10^{-6} M) containing the **1**-modified CdS nanoparticles, and a solution of **2**-functionalized CdS-nanoparticles. Inset: Kinetics of association of the first generation of the **2**-functionalized CdS nanoparticles with a) The **1**-modified Au/quartz interface that was hybridized with **2** (1×10^{-6} M) and then allowed to interact with **2**-functionalized CdS nanoparticles (1 mg mL^{-1}); b) the **1**-modified interface was hybridized with **3a** and then treated with **2**-functionalized CdS nanoparticles. B) Absorbance spectra (I) and fluorescence spectra (II) of layered oligonucleotide/DNA-cross-linked CdS nanoparticle arrays: a) to d) correspond to one to four CdS nanoparticle layers; $\lambda_{ex} = 405$ nm for fluorescence spectra.

  0044-8249/01/11310-1914 $ 17.50+.50/0

the absorbance and fluorescence spectra of the DNA-cross-linked CdS-nanoparticle arrays. The intensities of the absorbance and fluorescence spectra increase as the number of generations of cross-linked CdS particles increases. The large Stokes shift observed in the fluorescence spectra suggests that the emission originates from surface traps. In fact, the preparation of the CdS quantum dots involves the generation of an excess of Cd^{2+} surface sites to enable the association of the nucleic acid. These sites probably act as surface traps.

Figure 3 A shows the photocurrent action spectra upon the excitation of arrays that consist of different numbers of CdS nanoparticle generations which are associated with the

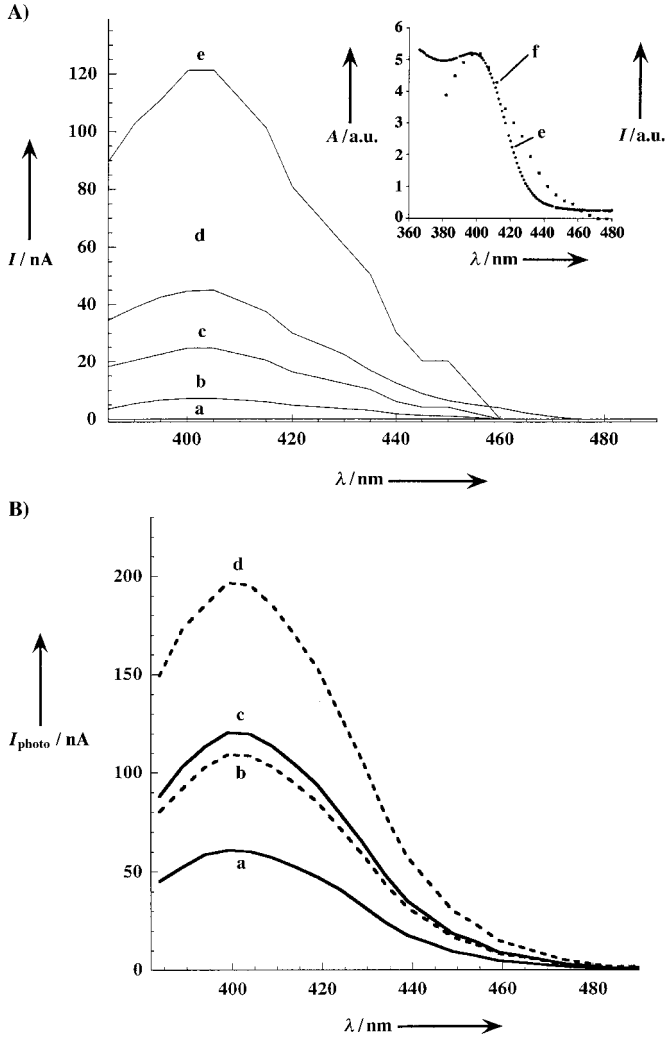

Figure 3. A) Photocurrent action spectra of an Au electrode that is associated with controlled numbers of layers of oligonucleotide/DNA-cross-linked CdS nanoparticles: a) Prior to the deposition of CdS nanoparticles. b) to e) One to four oligonucleotide/DNA-cross-linked CdS nanoparticle layers. Inset: Comparison of the photocurrent action spectrum of a four-layer CdS nanoparticle array (e) with the absorption spectrum (f) of the array. B) Photocurrent action spectra of two-layer (a) and four-layer (c) oligonucleotide-cross-linked CdS nanoparticle arrays. Two-layer (b) and four-layer (d) oligonucleotide/DNA-cross-linked CdS nanoparticle arrays in the presence of $[Ru(NH_3)_6]^{3+}$ (5×10^{-6} M). All photocurrent spectra were recorded under argon in 0.1 M KCl with triethanolamine (2×10^{-2} M) as sacrificial electron donor. The area of illuminated electrode corresponds to 1 cm^2. The photocurrent spectra were normalized with respect to the wavelength dependence of the light intensity.

electrode in the presence of triethanolamine (2×10^{-2} M) as a sacrificial electron donor. The photocurrent follows the absorbance spectrum of the CdS nanoparticles (Figure 3 A, inset), and it increases with increasing number of generations of cross-linked particles. As we use a sacrificial electron donor as hole scavenger, we attribute the resulting photocurrent to the injection of conduction-band electrons into the electrode. The photocurrent can be switched "on" and "off" by pulsed irradiation of the arrays. The mechanism of photocurrent generation probably involves the photoejection of conduction-band electrons of CdS particles in contact with or at tunneling distances from the electrode (cf. Figure 1). This suggests, however, that some of the cross-linked nanoparticles do not participate in the development of the photocurrent. To assist the generation of the photocurrent by inactive CdS particles, the arrays were treated with $[Ru(NH_3)_6]^{3+}$ (5×10^{-6} M), which binds electrostatically to the DNA.[27] The transition metal complex ($E^\circ = -0.16$ V vs SCE) acts as an electron acceptor for the conduction-band electrons ($E^\circ_{CB} < -0.9$ V vs SCE), and could thus mediate electron transfer from inactive CdS particles to the electrode.

Figure 3 B shows the photocurrents that are generated by the DNA-cross-linked CdS arrays that contain two and four generations of nanoparticles in the absence and presence of $[Ru(NH_3)_6]^{3+}$, respectively. In the presence of $[Ru(NH_3)_6]^{3+}$ the photocurrent is about twofold higher, and this implies that the DNA units act as a template for the electron-acceptor units that mediate electron transfer to the electrode (Figure 1). However, increasing the $[Ru(NH_3)_6]^{3+}$ concentration to 5×10^{-4} M adversely affects the photocurrent, which decreases to values below those observed for the CdS arrays without the electron acceptor. This result is reasonable, since at high bulk concentrations of $[Ru(NH_3)_6]^{3+}$, diffusional electron-transfer quenching of the semiconductor nanoparticles occurs. This process traps the conduction-band electrons and thus prevents even the direct electron photoejection process.

The photocurrents generated by the DNA-cross-linked array can be used for the quantitative detection of DNA. Figure 4 shows the photocurrents of a two-layer DNA-cross-linked nanoparticle array upon the formation of a third generation of CdS nanoparticles in the presence of **2**-functionalized CdS at different concentrations of **3**. As the concentration of **3** increases, enhanced photocurrents are observed owing to greater coverage of the electrode by the third generation of semiconductor nanoparticles. In all of the systems described in the present study, no photocurrents are observed upon interaction of the **1**-functionalized electrode with the **1**- or **2**-functionalized nanoparticles or on attempting to cross-link the nanoparticle arrays with **3a**. Hence, no nonspecific binding of the CdS nanoparticles to the transducers is observed, and the photocurrents are specific to the cross-linking process involving the target DNA **3**.

In conclusion, we have demonstrated the novel generation of photocurrents in controlled DNA-cross-linked semiconductor nanoparticle arrays. We revealed that the DNA cross-linking units act as a template for the association of $[Ru(NH_3)_6]^{3+}$ and the electrical wiring of the semiconductor with the electrode support. Other electron acceptors, and

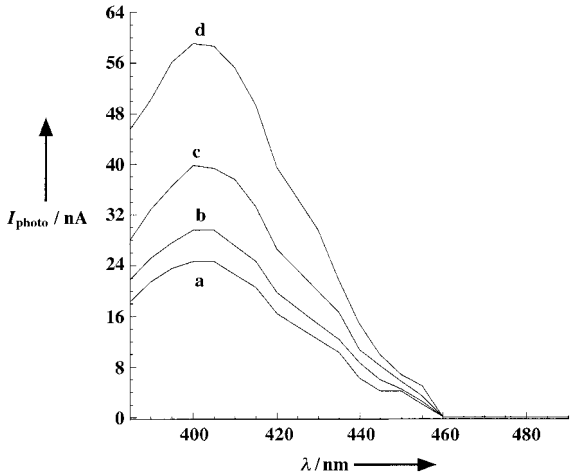

Figure 4. Sensing of the DNA **3** by means of the photocurrent response of the arrays. a) A two-layer oligonucleotide/DNA-cross-linked CdS array. b) Upon treatment of the two-layer cross-linked array with **3** (1×10^{-9} M) in the presence of **2**-functionalized CdS. c) Upon treatment of the two-layer cross-linked array with **3** (1×10^{-8} M) in the presence of **2**-functionalized CdS. d) Upon treatment of the two-layer cross-linked array with **3** (1×10^{-7} M) in the presence of **2**-functionalized CdS. Photocurrent spectra were recorded under the conditions specified in the caption of Figure 3.

specifically intercalators, could improve the electrical contact of the semiconductor particles with the electrode. The unique photophysical and photoelectrochemical properties of the semiconductor nanoparticles pave the way for new DNA sensors and electronic devices.

Experimental Section

Preparation of oligonucleotide-functionalized CdS nanoparticles: An AOT/*n*-heptane water-in-oil microemulsion was prepared by the solubilization of 2 mL of distilled water in 100 mL *n*-heptane in the presence of 7.0 g of AOT surfactant, dioctyl sulfosuccinate, sodium salt. The resulting mixture was separated into 60 mL and 40 mL reverse-micelle sub-volumes. Aqueous solutions of $Cd(ClO_4)_4$ (0.24 mL, 1M) and Na_2S (0.16 mL, 1.0M) were added to the 60 mL and 40 mL subvolumes of reverse micelles, respectively. After stirring the two subvolumes for 1 h, they were united and stirred under argon for 1 h to yield the CdS nanoparticles. To the resulting mixture were added aqueous solutions of 2-aminoethanethiol (cystamine; 0.17 mL, 0.32M) and 2-sulfanylethane sulfonic acid (0.33 mL, 0.32M), and the mixture was stirred for 24 h under Ar. The resulting mixture was evaporated under vacuum and the residue was successively washed with pyridine, *n*-heptane, acetone, and methanol to yield the cystamine/thioethanesulfonate-capped, water-soluble CdS nanoparticles.

The resulting CdS nanoparticles (1 mg mL^{-1}) were treated with the respective thiolated oligonucleotide (40–50 OD mL^{-1}), and the mixture was stirred for 24 h at room temperature under Ar. To the resulting mixture were added the appropriate salts to generate a 0.24M NaCl and 0.1M phosphate buffer solution (pH 7.4). The mixture was dialyzed for 48 h against 0.2M NaCl and 0.1M phosphate buffer (pH 7.4) containing 0.01% sodium azide. The resulting oligonucleotide-functionalized CdS nanoparticles exhibited high stability in the form of an aqueous suspension. The CdS nanoparticles could be isolated in the solid state by flash evaporation, and could be re-suspended in water for further experiments.

Characterization of CdS nanoparticles: To estimate the average number of oligonucleotide units associated with each CdS particle, a suspension of CdS nanoparticles was treated with the thiolated fluorescein-labeled oligonucleotide 5′-HS$(CH_2)_6$-GCGCGAACCGTA(T-fluorescein)A-3′, as described above. The resulting fluorescein-labeled, oligonucleotide-functionalized CdS (1 mg mL^{-1}, 200 μL) was treated for 2 h with DNase I (Amersham Pharmacia; 20 units at 37 °C in 40 mM tris HCl, pH 7.5, in the presence of 6 mM of $MgCl_2$). The resulting mixture was centrifuged, and the fluorescence of the fluorescence label in the supernatant solution was determined.

Independently, the capped CdS nanoparticles (1 mg) were heated for 2 h at 400 °C in an oven and then dissolved in perchloric acid. The content of Cd^{2+} in the sample was determined by atomic absorption. From the known amount of Cd^{2+} in the sample, the size of the CdS nanoparticles, the density of CdS, and the amount of fluorescence label released from the particles, we estimate that about 20–24 oligonucleotides are associated with each CdS particle.

Received: October 6, 2000
Revised: January 26, 2001 [Z15917]

[1] S. O. Kelley, J. K. Barton, *Science* **1999**, *283*, 375–381.
[2] M. Ratner, *Nature* **1999**, *397*, 480–481.
[3] F. D. Lewis, T. F. Wu, Y. F. Zhang, R. L. Letsinger, S. R. Greenfield, M. R. Wasielewski, *Science* **1997**, *277*, 673–676.
[4] H. W. Fink, C. Schonenberger, *Nature* **1999**, *398*, 407–410.
[5] E. Meggers, M. E. Michel-Beyerle, B. Giese, *J. Am. Chem. Soc.* **1998**, *120*, 12950–12955.
[6] J. Jortner, M. Bixon, T. Langenbacher, M. E. Michel-Beyerle, *Proc. Natl. Acad. Sci. USA* **1998**, *95*, 12759–12765.
[7] G. Hartwich, D. J. Caruana, T. de Lumley-Woodyear, Y. B. Wu, C. N. Campbell, A. Heller, *J. Am. Chem. Soc.* **1999**, *121*, 10803–10812.
[8] E. Braun, Y. Eichen, U. Sivan, G. Ben-Yoseph, *Nature* **1998**, *391*, 775–778.
[9] D. Porath, A. Bezryadin, S. de Vries, C. Dekker, *Nature* **2000**, *403*, 635–638.
[10] E. Ben-Jacob, Z. Hermon, S. Caspi, *Phys. Lett. A* **1999**, *263*, 199–202.
[11] C. A. Mirkin, R. L. Letsinger, R. C. Mucic, J. J. Storhoff, *Nature* **1996**, *382*, 607–609.
[12] J. J. Storhoff, C. A. Mirkin, *Chem. Rev.* **1999**, *99*, 1849–1862.
[13] N. C. Seeman, *Angew. Chem.* **1998**, *110*, 3408–3428; *Angew. Chem. Int. Ed.* **1998**, *37*, 3220–3238.
[14] J. Wang, X. H. Cai, J. Y. Wang, C. Jonsson, E. Palecek, *Anal. Chem.* **1995**, *67*, 4065–4070.
[15] H. Korri-Youssoufi, F. Garnier, P. Srivastava, P. Godillot, A. Yassar, *J. Am. Chem. Soc.* **1997**, *119*, 7388–7389.
[16] X. H. Cai, G. Rivas, P. A. M. Farias, H. Shiraishi, J. Wang, E. Palecek, *Electroanalysis* **1996**, *8*, 753–758.
[17] K. Hashimoto, K. Ito, Y. Ishimori, *Anal. Chem.* **1994**, *66*, 3830–3833.
[18] K. M. Millan, S. R. Mikkelsen, *Anal. Chem.* **1993**, *65*, 2317–2323.
[19] S. Takenaka, K. Yamashita, M. Takagi, Y. Uto, H. Kondo, *Anal. Chem.* **2000**, *72*, 1334–1341.
[20] D. J. Caruana, A. Heller, *J. Am. Chem. Soc.* **1999**, *121*, 769–774.
[21] F. Patolsky, E. Katz, A. Bardea, I. Willner, *Langmuir* **1999**, *15*, 3703–3706.
[22] F. Patolsky, A. Lichtenstein, I. Willner, *Angew. Chem.* **2000**, *112*, 970–973; *Angew. Chem. Int. Ed.* **2000**, *39*, 940–943.
[23] F. Patolsky, A. Lichtenstein, I. Willner, *J. Am. Chem. Soc.* **2000**, *122*, 418–419.
[24] F. Patolsky, K. T. Ranjit, A. Lichtenstein, I. Willner, *Chem. Commun.* **2000**, 1025–1026.
[25] T. A. Taton, R. C. Mucic, C. A. Mirkin, R. L. Letsinger, *J. Am. Chem. Soc.* **2000**, *122*, 6305–6306.
[26] R. Rossetti, J. L. Ellison, J. M. Gibson, L. E. Brus, *J. Chem. Phys.* **1984**, *80*, 4464.
[27] A. B. Steel, T. M. Herne, M. J. Tarlov, *Anal. Chem.* **1998**, *70*, 4670–4677.

  0044-8249/01/11310-1916 $ 17.50+.50/0